

W -boson production at upgraded HERA

M.N.Dubinin

*Institute of Nuclear Physics, Moscow State University
119899 Moscow, Russia*

H.S.Song

*Center for Theoretical Physics, Seoul National University
Seoul, 151-742, Korea*

Abstract

Event characteristics of W boson production at HERA collider are untrivial and sensitive to the production mechanisms. We analyse the distributions of the four particle final state defined by the complete set of W producing perturbative leading order diagrams in the Standard Model and its extension with the anomalous effective lagrangian in the gauge sector.

It is important to understand in details the mechanisms of W -boson production at upgraded HERA. The number of W -production events will be large enough both in leptonic and hadronic W decay channels, giving potentially large backgrounds to the signals of new physics [1], such as contact interactions, leptoquarks and R -parity conserving or violating SUSY processes. At the same time the single W production is influenced by γWW and ZWW vertices that still are not precisely measured. While the weak current couplings of gauge bosons are measured with the accuracy of 10^{-4} [2], the accuracy of anomalous couplings restriction in the gauge boson sector from the Tevatron data is around 0.5 (in units of dimensionless parameters κ , λ) only ([3], see also [4]), so the self-interaction of vector bosons is not experimentally fixed at comparable level of precision.

W boson production in the electron-proton mode can be observed in the main channel $e^-p \rightarrow e^- \mu^+ \nu_\mu X$ and maybe a few events $e^-p \rightarrow \nu_e \mu^+ \bar{\nu}_\mu X$ can be reconstructed. Positron-proton mode $e^+p \rightarrow e^+ \mu^+ \nu_\mu X$ has practically the same total rate and event characteristics, because the Feynman graph

topology of the positron-proton mode is different only for some W and Z exchange weak diagrams giving the contributions that are small in comparison with the dominant t -channel photon exchange diagrams. The complete set of 10 tree level diagrams for the main process of W -boson production $e^-p \rightarrow e^- \mu^+ \nu_\mu X$ is shown in Fig.1. In the simpler $2 \rightarrow 3$ process approximation [5] of W -boson on-shell $M_{\mu\nu} = (p_\nu + p_\mu)^2 = m_W^2$ we have to keep seven s -channel diagrams with an outgoing W boson line and omit ladder diagrams 1,6 and 7. However this approximation of infinitely small W width $m_W \Gamma_{tot}/[(M_{\mu\nu}^2 - m_W^2)^2 + m_W^2 \Gamma_{tot}^2] = \delta(M_{\mu\nu} - m_W)$, being rather satisfactory for the calculation of total W production rate, is not sufficient for the analysis of some specific features of event topology, like particle distributions from the multiperipheral mechanisms. Taking W boson off-shell $W \rightarrow \mu \nu_\mu$ in the $2 \rightarrow 4$ process approximation requires ladder graphs 1,6,7 in order to preserve gauge invariance [6].

Main contribution to the cross section comes from the diagram 3 containing photon and quark t -channel propagators. When the t -channel gamma and quark are close to mass shell the QCD corrections are large, potentially developing a nonperturbative regime of 'resolved photon' [7]. The kinematical configurations of resolved photon are usually separated by a cut near the u -channel quark pole $\Lambda^2 = -(p_q - p_W)^2$. Resolved W -production is not more than a quark-antiquark fusion where one of the quarks appears as a constituent of gamma and another one as a constituent of proton. Existing parametrizations of quark distributions inside gamma (measured in a relatively low Q^2 $\gamma\gamma$ collisions and then extrapolated to the region of $Q^2 \sim m_W^2$), seem to be not as precise as PDF in proton, so the resolved W -production cannot be calculated with the same reliability [8] as the perturbative leading order (also called 'direct') contribution of ten diagrams in Fig.1. Double counting of the perturbative part of the photon structure function and the collinear configuration of the direct process amplitude is removed by the subtraction of LO $\gamma \rightarrow qq'$ splitting term. Resulting contribution of the resolved part is of order 10% of the W -production cross section.

Alternative method of the resolved part separation by a cut near the t -channel gamma pole $Q^2 = -(p_e - p'_e)^2$ [9] uses a delicate application of the equivalent gamma approximation to the subprocess with t -channel quark $\gamma q \rightarrow q' W^*$. In this case by definition of [9] the main 'direct' (or 'photoproduction') contribution comes from a configuration with the quasireal gamma and electron at a small angle θ_e with the beam. The $2 \rightarrow 3$ amplitude with $\theta_e \geq 5$ deg. (seven diagrams of Fig.1, W on-shell) corresponds to 'DIS contribution'. Ladder diagrams are omitted. Resolved photon contribution

becomes dominant in the framework of this method. Important role of the NLO QCD corrections to the resolved part $q'q \rightarrow W$, giving the enhancement of it by about 40%, is demonstrated by an explicit calculation.

In the following we shall discuss the distributions corresponding to direct (perturbative leading order) part of the W production amplitude in the Standard Model and beyond [8]. Resolved gamma is separated by a Λ^2 cut.

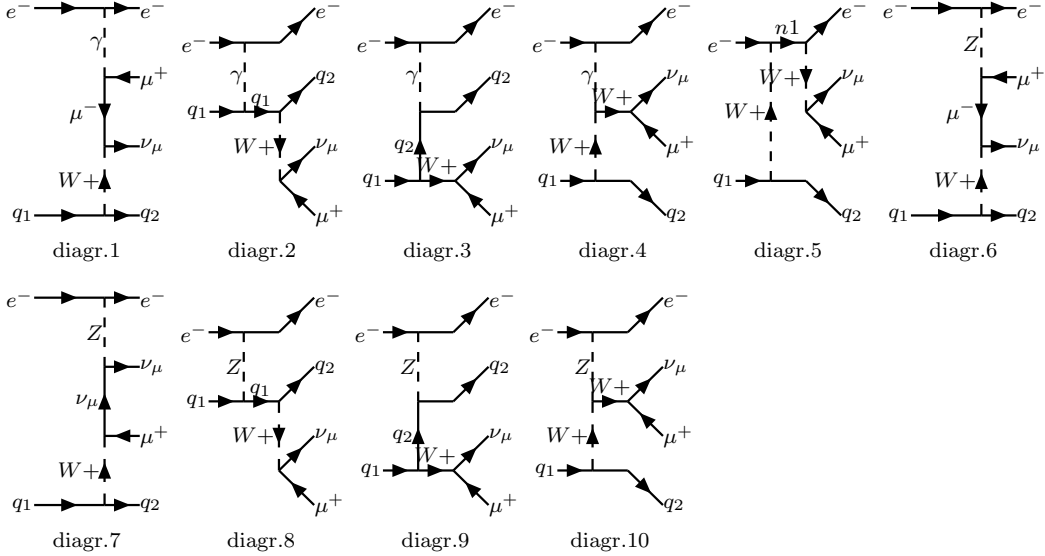


Figure 1: Feynman diagrams for the process $e^- q_1 \rightarrow e^- \mu^+ \nu_\mu q_2$

Calculation of the leading order amplitude (ten diagrams in Fig.1) was performed by means of CompHEP package [10]. We used the 'overall' prescription [11, 6] for vector boson propagators. Electron mass was kept nonzero for the regularization of t -channel gamma pole. Numerical level cancellation of the $1/Q^4$ gamma propagator pole in the separately taken squared diagrams to the $1/Q^2$ pole in the entire amplitude, required by the gauge invariance, can be demonstrated explicitly [8].

We show the event characteristics of the process $e^- p \rightarrow e^- \mu^+ \nu_\mu X$ in Figs.2-4 (proton structure functions MRS A [12]). First row of plots in each figure represents the distributions of the electron, second row of plots - distributions of the (anti)muon, and third row of plots shows the distributions of the final quark (all partonic subprocesses contributing to W production are summed). Different cuts for t -channel quark momentum $\Lambda^2 = -(p_q - p_W)^2$ were imposed for the calculation of event characteristics in Fig.2 and Fig.3, where Λ is equal to 0.2 GeV and 5 GeV, correspondingly. The distributions in

	EPVEC		CompHEP	
	e^+p	e^-p	e^+p	e^-p
Λ cut 0.2 GeV, no W pole cut				
MRS A	71.7	70.8	93.1	92.1
CTEQ4L	71.5	70.8	93.0	91.9
Λ cut 5 GeV, no W pole cut				
MRS A	50.7	49.5	68.9	68.6
CTEQ4L	50.9	49.9	69.1	68.9
Λ cut 5 GeV, W pole cut ± 20 GeV				
MRS A	44.2	43.2	53.6	51.7
CTEQ4L	44.5	43.4	53.7	51.9

Table 1: EPVEC and CompHEP total rates (fb) for the processes $e^+p \rightarrow e^+\mu^+\nu_\mu X$ and $e^-p \rightarrow e^-\mu^+\nu_\mu X$ Direct part only, proton structure functions MRS A [12] and CTEQ4L [13]. Parton distribution functions factorisation scale m_W , resolved gamma region is separated by a Λ cut.

Fig.4 were calculated at $\Lambda = 5$ GeV with the phase space cut 20 GeV around the W pole: $M_W - 20 \text{ GeV} \leq M(\mu\nu_\mu) \leq M_W + 20 \text{ GeV}$. This cut is used in the EPVEC generator [6], so the distributions in Fig.4 are calculated using the phase space cuts similar to the cuts used in [14]. Additional phase space cuts in the EPVEC that were introduced to ensure the numerical stability of the muon pole integration in the ladder diagram 1, Fig.1, lead to the EPVEC total rate regularly smaller than the CompHEP total rate, where the muon pole region is exactly integrated (see Table 1).

Soft muons in the distributions $d\sigma/dE_\mu$ and $d\sigma/dp_{T\mu}$ come from the ladder diagrams 1,6,7 in Fig.1. Jets at the angle 180 degrees with the proton beam appear from diagram 3, Fig.1, when the quasireal photon produces a quark-antiquark pair collinear to the initial electron. We can see that the backscattered jet peak is sensitive to the value of Λ cut and gradually goes down as we increase it. But this decrease of direct contribution should be compensated by the 'photon remnant' in the contribution from the resolved part. Muons at 180 degree with the proton beam from the ladder diagrams appear at any value of Λ - only the shape of $d\sigma/dE_\mu$ is slightly affected and the normalization is changed. Kinematical cut around the W -pole implemented in 'canonical' EPVEC removes soft muons and muons at 180 degree with the beam completely. It is interesting to notice that the four-fermion

final state configurations with backscattered soft muons are observed in the simulation for LEP2 [15], where in the channel $e^+e^- \rightarrow e^-\bar{\nu}_e\mu^+\nu_\mu$ diagram topologies are the same (if we replace the quark line by the electron line).

In the muonic channels the total cross section is equal approximately to 150-160 fb, giving about 35 events/year at the integrated luminosity 200 pb^{-1} . Additional kinematical cuts are necessary in the electron channels for separation of misidentification backgrounds, and the number of identifiable events from $W \rightarrow e\nu_e$ is slightly smaller. In total at upgraded HERA collider it could be possible to observe about 60 W -production events/year. At present time HERA luminosity is too small to produce a number of W sufficient for a quantitative analysis. Presently available H1 data [16] shows one event in the electron channel (2.4 events expected) and two events in the muon channel (0.8 events expected), with the topology compatible with W production processes (three more H1 events in the muon channel have the kinematic properties different from those given by W production mechanisms). ZEUS data [17] shows three events in the electron channel and none of the events passes through kinematical cuts in the muon channel. Detailed discussion can be found in [18].

Anomalous U(1) gauge invariant, C and P parity conserving effective lagrangian in the gauge sector can be taken in the form [19]

$$L_{eff} = g_V(W_{\mu\nu}^+W^{\mu\nu}V^\nu - W^{\mu\nu}W_\mu^+V_\nu + \kappa W_\mu^+W_\nu V^{\mu\nu} + \frac{\lambda}{m_W^2}W_{\rho\mu}^+W_\nu^\mu V^{\nu\rho}) \quad (1)$$

where $g_\gamma = e$ and $g_Z = e \cos\vartheta_W / \sin\vartheta_W$, $W_{\mu\nu} = \partial_\mu W_\nu - \partial_\nu W_\mu$, $V_{\mu\nu} = \partial_\mu V_\nu - \partial_\nu V_\mu$. and λ, κ are dimensionless parameters. Following the tradition the value of λ is expressed in the units of m_W . We show one of the distributions calculated using the anomalous effective lagrangian (1) in Fig.5.

Taking into account some typical detector experimental cuts necessary for the separation of misidentification backgrounds and realistic experimental acceptancies [14] we can estimate the following limits [8] for $\Delta\kappa$ and λ , giving the observable deviation of total cross section from the Standard Model value at 68% and 95% confidence level:

$$\begin{aligned} -1.70 < \lambda < 1.70, & \quad -1.05 < \Delta\kappa < 0.48, & \quad 68\% \quad CL \\ -2.24 < \lambda < 2.24, & \quad \Delta\kappa < 0.89, & \quad 95\% \quad CL \end{aligned}$$

at the integrated luminosity 200 pb^{-1} , and

$$\begin{aligned} -1.03 < \lambda < 1.03, & \quad -0.31 < \Delta\kappa < 0.27, & \quad 68\% \quad CL \\ -1.75 < \lambda < 1.75, & \quad -0.58 < \Delta\kappa < 0.46, & \quad 95\% \quad CL \end{aligned}$$

at the integrated luminosity 1000 pb^{-1} . The limits from Tevatron collider available at present time [3] are close to the possible upgraded HERA limits at the luminosity 1000 pb^{-1} .

M.D. is grateful to M.Spira, M.Kuze and D.Zeppenfeld for useful discussions and he thanks very much C.Diaconu and D.Waters for help in the comparison of EPVEC and CompHEP results.

References

- [1] H1 Collaboration, ICHEP98, XXIX Int. Conf. on High Energy Physics, Vancouver, 23-29 July 1998, abstracts 579, 580, 581, 584
ZEUS Collaboration, ICHEP98, XXIX Int. Conf. on High Energy Physics, Vancouver, 23-29 July 1998, abstracts 753, 754, 758, 759
- [2] Particle Data Group, Phys.Rev. D54 (1996) 1
- [3] S.Abachi et al, D0 Collaboration, Phys.Rev.Lett., 78 (1997) 3634
- [4] D.Schildknecht, Acta Phys. Pol., B28 (1997) 2291
- [5] U.Baur, D.Zeppenfeld, Nucl.Phys. B325 (1989) 253
- [6] U.Baur, J.Vermaseren, D.Zeppenfeld, Nucl.Phys. B375 (1992) 3
- [7] M.Drees, Mod.Phys.Lett., A2 (1987) 573
J.Blümlein, G.Schuler, in: *Proc. of Snowmass Summer Study on Research Directions for the Decade*, 1990
- [8] M.N.Dubinin, H.S.Song, Phys.Rev. D57 (1998) 2927
- [9] P.Nason, R.Rueckl, M.Spira, in: Proc. of the 3rd Phenomenology Workshop on HERA Physics, Durham, 1998 (hep-ph/9902296)
- [10] E.Boos, M.Dubinin, V.Ilyin, A.Pukhov, V.Savrin, preprint INP MSU 94-36/358, 1994 (hep-ph/9503280)
in: *Proc. of X Workshop on High Energy Physics and Quantum Field Theory*, ed.by B.Levtchenko, V.Savrin, Moscow, 1996, p.101
see also <http://theory.npi.msu.su/~comphep>
- [11] Y.Kurihara, D.Perret-Gallix, Y.Shimizu, Phys. Lett., B349 (1995) 367
- [12] A.D.Martin, W.J.Stirling, R.G.Roberts, Phys.Rev. D51 (1995) 4756

- [13] H.L.Lai, J.Huston, S.Kuhlmann, F.Olness, J.Owens, D.Soper, W.K.Tung, H.Weerts, Phys.Rev. D55 (1997) 1280
- [14] V.Noyes, in: *Proc.of the Workshop on Future Physics at HERA 1995/96*, ed.by G.Ingelman, A.De Roeck and R.Klanner, p.190
- [15] R.Tanaka, CPP meeting, December 1998, Tokyo, see <http://alephwww.cern.ch/~tanakar/>
A.Kounine, LEP2 Workshop meeting, March 1999, CERN, see <http://www.to.infn.it/~giampier/lep2.html>
- [16] H1 Collaboration, ICHEP98, XXIX Int. Conf. on High Energy Physics, Vancouver, 23-29 July 1998, abstract 578
H1 Collaboration, DESY preprint 98-063
- [17] ZEUS Collaboration, ICHEP98, XXIX Int. Conf. on High Energy Physics, Vancouver, 23-29 July 1998, abstract 756
- [18] C.Diaconu, J.Kalinowski, T.Matsushita, H.Spiesberger, D.Waters, hep-ph/9901335
M.W.Krasny, H.Spiesberger, hep-ph/9901359
- [19] K.Hagiwara, R.D.Peccei, D.Zeppenfeld, K.Hikasa, Nucl.Phys. B282 (1987) 253

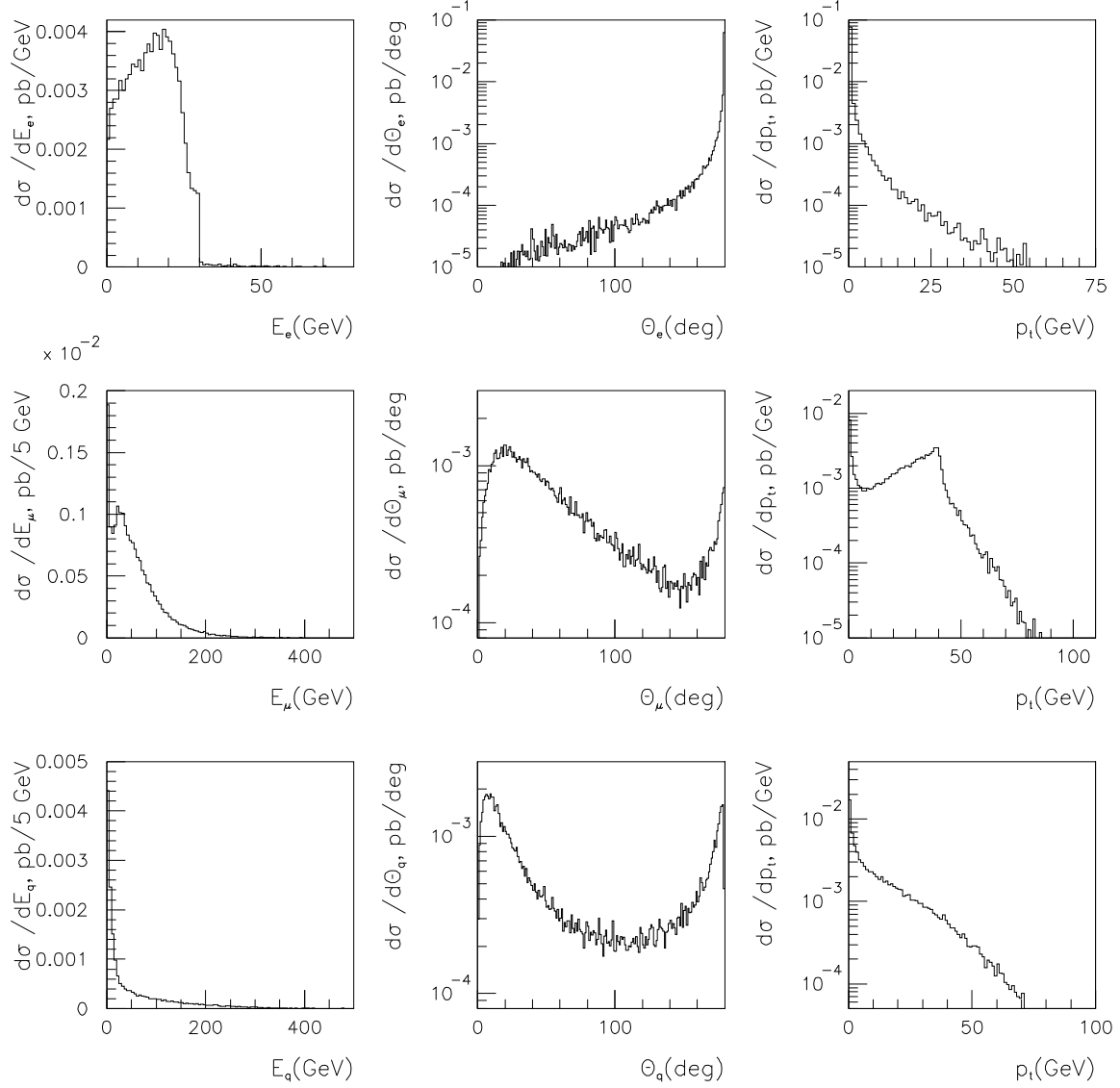


Figure 2: First row of plots - distributions of the electron energy, scattering angle and transverse momentum in the process $e^-p \rightarrow e^-\mu^+\nu_\mu X$. Second row of plots - distributions of the muon energy, muon scattering angle and transverse momentum. Third row of plots - distributions of the quark energy, angle and transverse momentum for the same process. Total cross section 92.1 fb, t -channel quark cut $\Lambda = 0.2$ GeV.

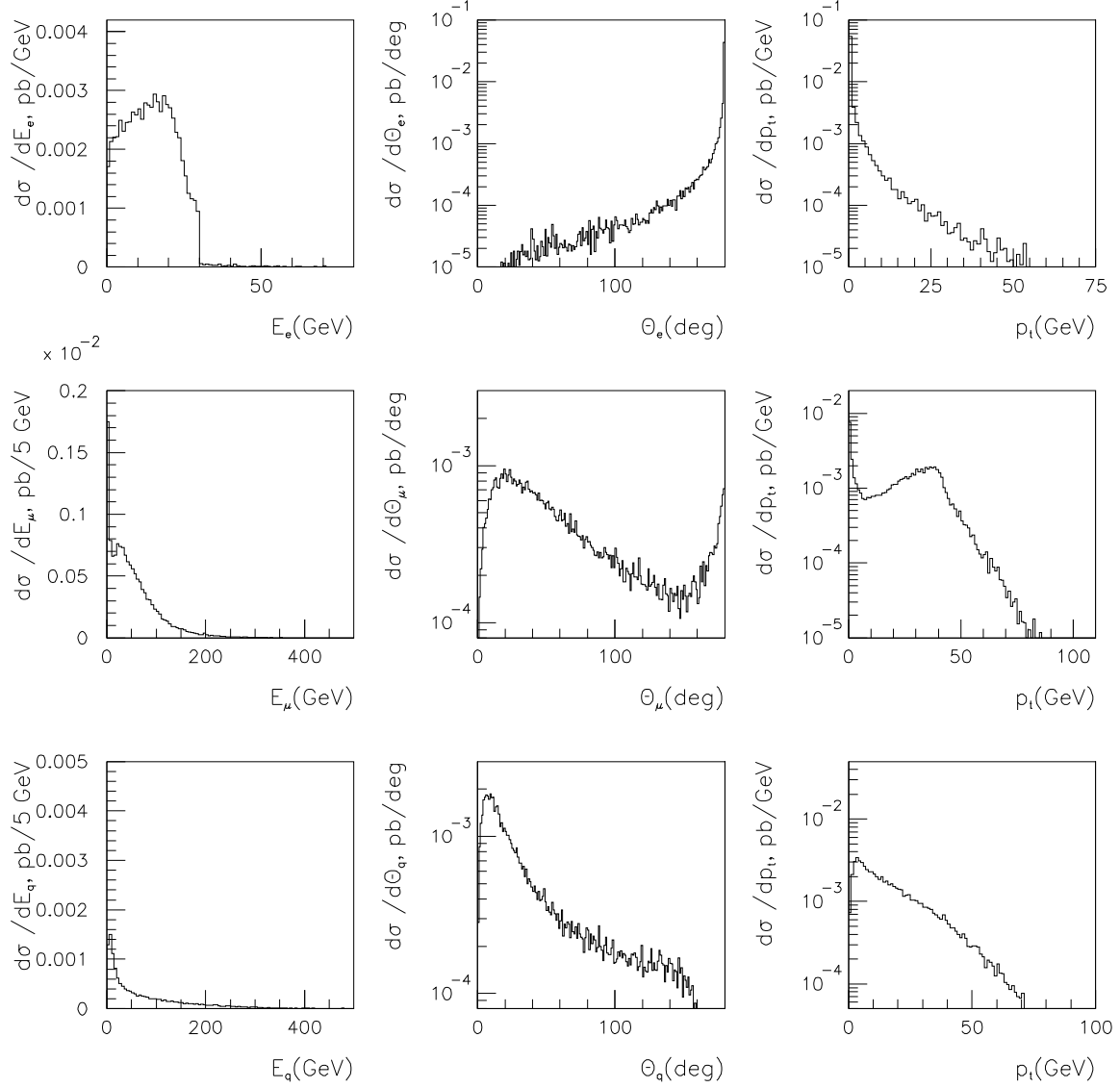


Figure 3: First row of plots - distributions of the electron energy, scattering angle and transverse momentum in the process $e^-p \rightarrow e^-\mu^+\nu_\mu X$. Second row of plots - distributions of the muon energy, muon scattering angle and transverse momentum. Third row of plots - distributions of the quark energy, angle and transverse momentum for the same process. Total cross section 68.6 fb, t -channel quark cut $\Lambda = 5$ GeV.

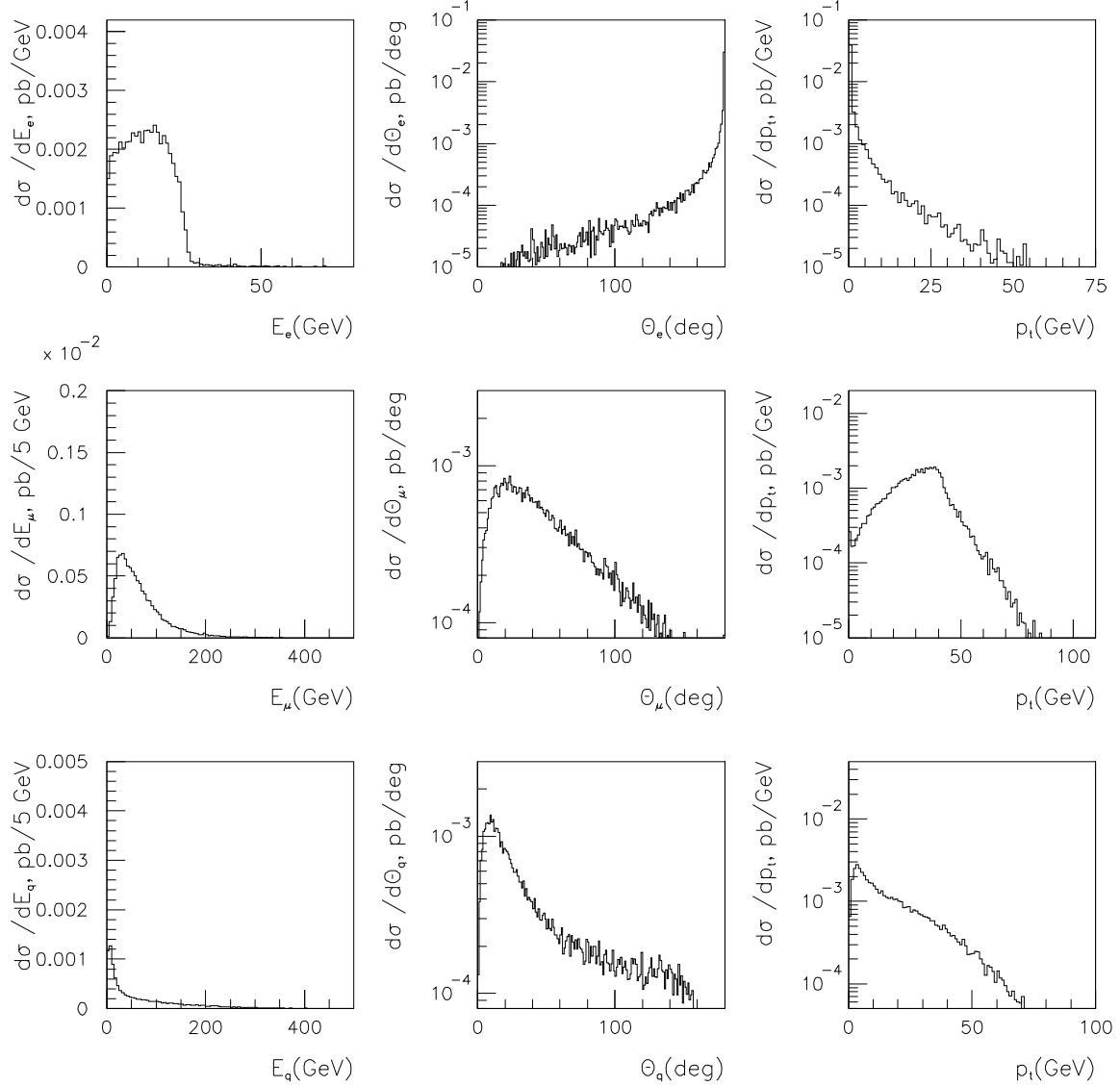


Figure 4: First row of plots - distributions of the electron energy, scattering angle and transverse momentum in the process $e^-p \rightarrow e^-\mu^+\nu_\mu X$. Second row of plots - distributions of the muon energy, muon scattering angle and transverse momentum. Third row of plots - distributions of the quark energy, angle and transverse momentum for the same process. Total cross section 51.7 fb, t -channel quark cut $\Lambda = 5$ GeV, the cut around the W pole 20 GeV, to be compared with the same distributions obtained by means of EPVEC generator, see [14]

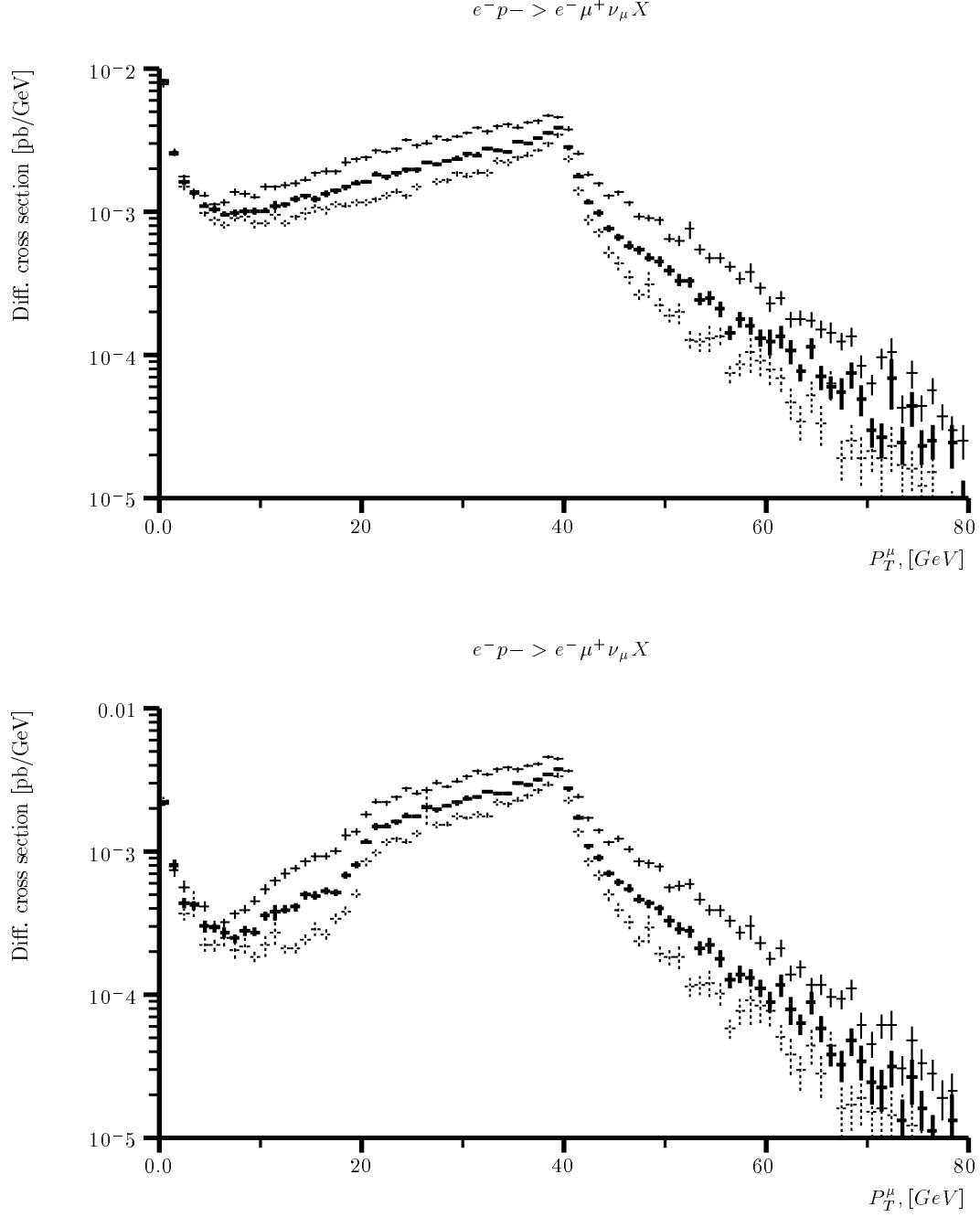


Figure 5: Distribution of muon transverse momentum in the reaction $e^- p \rightarrow e^- \mu^+ \nu_\mu X$. Upper plot: no kinematical cuts, solid lines - standard case, dash lines - anomalous three vector boson couplings case, $\lambda = 0$, $\kappa = 0$, thin solid lines - $\lambda = 0$, $\kappa = 2$. Lower plot: the same distributions after the detector kinematical cuts $E_\mu \geq 10$ GeV, missing $p_T \geq 20$ GeV.